CHIN. PHYS. LETT. Vol. 37, No. 5 (2020) 054301

# Tunable Double-Band Perfect Absorbers via Acoustic Metasurfaces with Nesting Helical Tracks *

Shu-Huan Xie(解书欢)[1†], Xinsheng Fang(房鑫盛)[2†], Peng-Qi Li(李鹏奇)[1], Sibo Huang(黄思博)[2], Yu-Gui Peng(彭玉桂)[1], Ya-Xi Shen(沈亚西)[1], Yong Li(李勇)[2**], Xue-Feng Zhu(祝雪丰)[1**]

[1]*School of Physics and Innovation Institute, Huazhong University of Science and Technology, Wuhan 430074*
[2]*Institute of Acoustics, School of Physics Science and Engineering, Tongji University, Shanghai 200092*

(Received 9 February 2020)

*We propose a design of tunable double-band perfect absorbers based on the resonance absorption in acoustic metasurfaces with nesting helical tracks and deep-subwavelength thicknesses ($< \lambda/30$ with $\lambda$ being the operation wavelength). By rotating the cover cap with an open aperture on the nesting helical tracks, we can tailor the effective lengths of resonant tubular cavities in the absorber at will, while the absorption peak frequency is flexibly shifted in spectrum and the acoustic impedance is roughly matched with air. The simulated particle velocity fields at different configurations reveal that sound absorption mainly occurs at the open aperture. Our experiment measurements agree well with the theoretical analysis and simulation, demonstrating the wide-spectrum and tunable absorption performance of the designed flat acoustic device.*

*PACS:* 43.35.+d, 43.20.+g, 43.40.+s DOI: 10.1088/0256-307X/37/5/054301

Sound absorption is significant in room acoustics (e.g., noise elimination). In the past few decades, dark acoustic metamaterials have been extensively explored, including configurations such as porous structures,[1] decorated membrane resonators,[2–4] hybrid resonators,[5–7] plate-type metamaterials,[8] and Helmholtz resonators.[9] Those resonant structures that support enhanced acoustic energy density at the resonance frequencies are demonstrated to be very promising in low-frequency sound absorption (<500 Hz) because conventional sound absorbing materials, such as plastic foam, fiber glass and mineral wool, have much lower dissipation coefficients under long wavelength conditions due to nontrivial wave diffraction.[10] However, based on linear acoustic theory, these resonant structures have sizes comparable with the operation wavelength.[11] For example, for the Fabry–Pérot resonators, the tube cavity length is around one quarter of the resonance wavelength. Consequently, the resonator-based sound absorbers will have bulky volumes of tens of centimeters in thickness for the low-frequency airborne sound (<500 Hz or $\lambda > 0.7$ m). Moreover, there is another severe issue for the resonator-based sound absorbers—that is, the trade-off golden law for the resonance process. Nontrivial sound absorption is associated with the resonance process, which is narrow band in nature for high-quality resonators.

In this Letter, we present a wide-band and tunable double-band perfect absorber with a three-dimensional (3D) space-coiling structure and deep-subwavelength fingerprint. Here the double-band perfect absorption is enabled through integrating different resonant structures into a unit cell. One intuitive approach is by coiling up the space. As pointed out in previous works, space coiling can be utilized to construct metamaterials with counterintuitive parameters,[12,13] such as single-negative/double-negative metamaterials,[14,15] zero-index metamaterials[16] and extremely high refractive-index metamaterials.[15–18] Those extreme material parameters are always complex numbers, where the imaginary parts denote the inherent loss or energy absorption. Note that the zigzag or spiral paths will further enhance the absorption by increasing the length of viscous boundary layers.[9] Two-dimensional space coiling still has some limitations in broadband applications[9,19–21] because the lateral dimension increases in the case of tightly packing different structures into one unit cell, which in turn will degrade the overall performance of the metasurface device. A similar limitation may also occur in 3D space coiling structures. The degradation of the overall performances in 2D/3D space coiling structures can be improved by adjusting the design of the structures. In this work, we use helical structured 3D space coiling to pack different resonators into one unit-cell with a high space utilization and moderate lateral dimension. The thickness of the 3D space-coiling structure is on a deep-subwavelength scale ($<\lambda/30$ with $\lambda$ the

*Supported by the National Natural Science Foundation of China (Grant Nos. 11674346, 11704284, 11690030, and 11690032). Xue-Feng Zhu and Shu-Huan Xie were supported by the Bird Nest Plan of HUST.

†Shu-Huan Xie and Xinsheng Fang contributed equally to this work.

**Corresponding author. Email: yongli@tongji.edu.cn; xfzhu@hust.edu.cn

© 2020 Chinese Physical Society and IOP Publishing Ltd

operation wavelength). Furthermore, we implement a wide-range change of absorption bands by adjusting the effective length of the 3D space-coiling helical tracks.[22,23] During the tuning process, we find that the acoustic impedance of the absorber is always roughly matched with the background air, leading to a good absorption area flexibly shifting in a wide frequency spectrum.

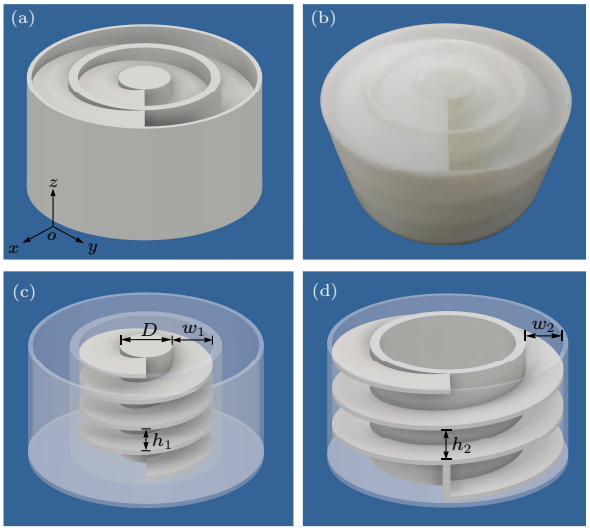


**Fig. 1.** (a) Schematic diagram of the double-band perfect absorber unit cell with a 3D space-coiling structure. (b) The experiment sample fabricated by the 3D printing technology. (c) Schematic of the inner helical track. (d) The schematic of the outer helical track.

Figure 1(a) presents a schematic of the double-band perfect absorber, which is a nesting 3D space-coiling structure. We fabricated the experiment sample using the 3D printing technology via the laser sintering stereo-lithography with photosensitive resin, as shown in Fig. 1(b). The outer diameter of the cylindrical sample is designed to be 100 mm, which is matching to the cross-sectional size of commercial impedance tubes. In addition, the thickness of the sample is designed to be less than one thirtieth of the operation wavelength ($<\lambda/30$). The 3D space-coiling structure takes the form of helical tracks. Figures 1(c) and 1(d) show the schematics of the inner and outer helical tracks. The geometric parameters are denoted in the figures, where the pitch of the inner helical track $h_1 = 10$ mm, the width of the inner helical track $w_1 = 17$ mm, and the diameter of the supporting pole $D = 22$ mm. For the outer helical track, the pitch $h_2 = 14$ mm and the width $w_2 = 15.5$ mm. Basically, more resonant structures can be tightly packed into one unit cell by twining additional helical tracks with different pitches and widths around the supporting pole. In the proof-of-concept experiments, we focus on the case of two different helical tubular cavities for simplicity.

As shown in Fig. 1, the nesting 3D space-coiling structure can be regarded as two air tubes with rigid back walls and variable sections. On the basis of acoustic principle, for a tube with a rigid back wall, the acoustic impedance at the opening aperture is

$$Z = -i\frac{\rho c}{S}\cot(kL), \tag{1}$$

where $S$ and $L$ are the cross-sectional area and length of the air tube; $\rho$ and $c$ are the effective mass density and sound velocity inside the tube; $k$ is the effective wave number for sound waves propagating inside the tube. For narrow tubes, the viscous and thermal conduction effects cannot be ignored. At the solid surface, the boundary conditions can be expressed into zero particle velocity and zero temperature gradient, which results in large relative motion within the viscous boundary layer and thus the breakdown of the adiabatic character of sound wave propagation.[24] Based on the Kirchhoff theory, in narrow tubes, the effective mass density, the sound velocity and the wave number have imaginary parts and are related to the shape and area of the cross section.[25] In our case, the helical air tubes have variable sections, so that the surface impedance can hardly be calculated analytically. In the following, we use the finite element solver COMSOL Multiphysics 5.3$^{\mathrm{TM}}$ to numerically calculate the surface impedance at the aperture and the absorption coefficient of the helical metamaterial. We imposed the acoustic pressure module, thermo-viscous module and structural mechanics module to free space, helical air tubes and solid helix structure, respectively. Solid-fluid interaction was set at the boundaries between air and solids.

For a sound absorber, the relation between the surface impedance and the reflection coefficient is[24]

$$C_{\mathrm{r}} = \frac{Z\cos(\theta) - \rho_0 c_0}{Z\cos(\theta) + \rho_0 c_0}, \tag{2}$$

where $Z$ represents the surface impedance, the reflection coefficient $C_{\mathrm{r}}$ denotes the pressure ratio of reflected sound to incident sound, $\theta$ is the incident angle of sound waves, $\rho_0$ and $c_0$ are the mass density and sound velocity in air. For our designed sample, the surface impedance $Z$ can be calculated by the acoustic resistance $x_{\mathrm{s}}$ and reactance $y_{\mathrm{s}}$, by the relation

$$Z = (x_{\mathrm{s}} + iy_{\mathrm{s}})\rho_0 c_0, \tag{3}$$

where $x_{\mathrm{s}}$ and $y_{\mathrm{s}}$ are normalized to the air impedance. For the absorber, the absorption coefficient $\alpha = 1 - |C_{\mathrm{r}}|^2$, which, from Eqs. (2) and (3), is also expressed as

$$\alpha = \frac{4x_{\mathrm{s}}}{(1 + x_{\mathrm{s}})^2 + y_{\mathrm{s}}^2}. \tag{4}$$

For the normal incidence ($\theta = 0°$), unitary absorption occurs under the condition of impedance matching at the sample surface, i.e., $Z = \rho_0 c_0$. In this case, the normalized acoustic resistance and reactance are

$x_s = 1$ and $y_s = 0$, respectively. In the following, we experimentally investigate the absorption coefficient, acoustic resistance and reactance of the designed 3D space-coiling structure.

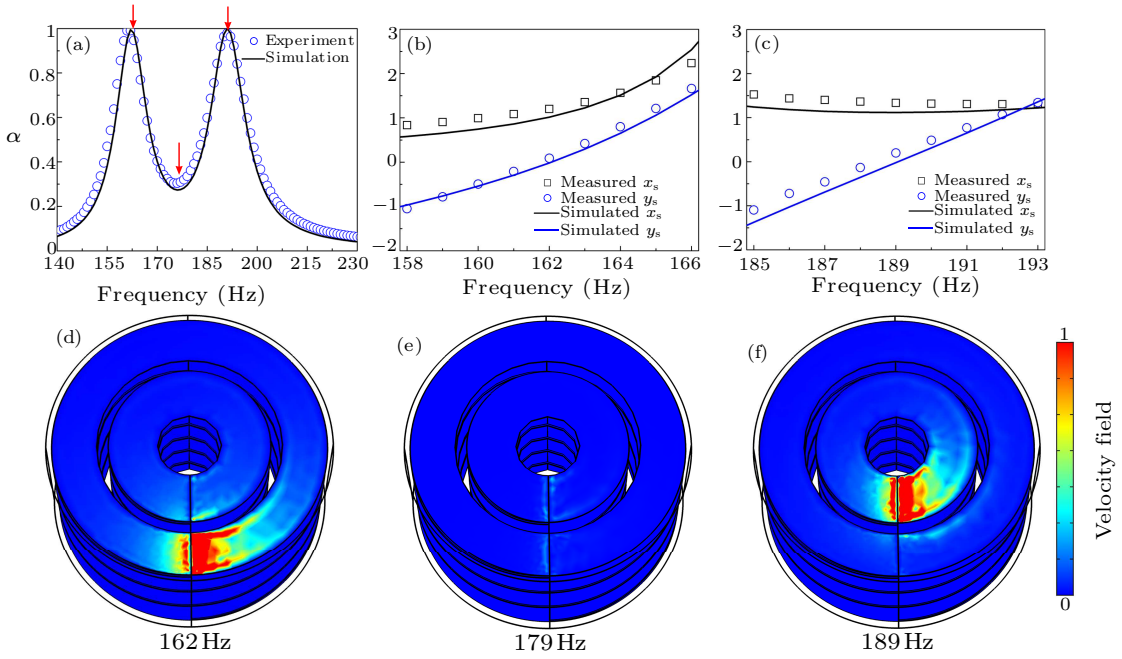


**Fig. 2.** (a) Measured and simulated absorption coefficient $\alpha$ in the frequency range from 140 Hz to 230 Hz. [(b), (c)] Measured and simulated specific acoustic resistance $x_s$ and acoustic reactance $y_s$ from 158 Hz to 166 Hz and from 185 Hz to 193 Hz, respectively. The acoustic resistance and reactance of absorbers are normalized with respect to the ones of air. [(d), (e), (f)] Simulated particle velocity fields of sound at the frequencies of 162 Hz, 179 Hz and 189 Hz, respectively, as marked by the arrows in (a).

The absorption spectrum is shown in Fig. 2(a), where the measured and simulated data agree well with each other. In experiments, the measurement of the absorption coefficient was conducted using a commercial impedance tube (Brüel & Kjær type-4206T, diameter-100 mm), where a pair of condenser microphones (Brüel & Kjær type-4187, 1/4-inch) were used at designated positions to extract the amplitude and the phase of the acoustic pressure field. The white-noise sound source is powered by the amplifier (Brüel & Kjær type-2734). From Fig. 2(a), unitary sound absorption occurs at 162 Hz and 189 Hz. In Figs. 2(b) and 2(c), we show the measured acoustic resistance $x_s$ and reactance $y_s$ in the frequency ranges of interest, respectively. These results demonstrate that perfect sound absorption corresponds to the case that $x_s = 1$ and $y_s = 0$. In this case, the absorber is purely resistive and the reactance is completely suppressed. We further calculate the velocity fields in the absorber unit cell to reveal the physical mechanism of sound absorption in the meta-structure. Figures 2(d)–2(f) show the simulated particle velocity fields at different frequencies of 162 Hz, 179 Hz and 189 Hz, where the corresponding absorption coefficients are marked by the arrows in Fig. 2(a). From simulations, we find that the local resonances play a major role in the perfect sound absorption, where the resonance-induced velocity fields will trigger nontrivial relative motion within the viscous boundary layer.[26] Internal friction thus transforms the acoustic energy into heat dissipation. At resonance frequencies of 162 Hz and 189 Hz, we observe that the regions of large particle velocity fields locate mainly at the apertures of outer helical track and inner helical track, respectively, as revealed in Figs. 2(d) and 2(f). It indicates two important guiding rules for implementing tunable acoustic devices. One is that the maximum absorption strength depends on the aperture. The other is that the effective length of the coiling tube mainly determines the perfect absorption frequency. Based on the guiding rules, it is intuitive to come up with a tunable configuration of sound absorbers.

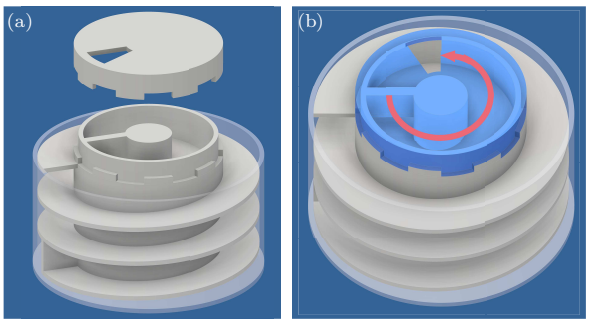


**Fig. 3.** (a) The schematic diagram of the tunable double-band perfect absorber unit cell. (b) The case when the cover cap with an open aperture is rotated by 270°.

Figure 3(a) shows a schematic diagram of the tun-

able sound absorber unit cell. A rotatable cover cap with a fan-like aperture enables the tunable functionality of the metasurface device. The periodic slots are utilized to perfectly seal the air inside the helical structure and prevent possible sound leakage, so that the absorption efficiency could reach unitary at local resonances. Rotating the cap will change the effective length of the inner coiling tube and thus shift the absorption band in a wide frequency range. Specifically, when the cover rotates by 270°, as shown in Fig. 3(b), the effective length is increased by around 70 mm in the designed structure, as marked by the arrow, which will make the absorption band redshift markedly. In the proof-of-concept experiment, we only shift one absorption band with the other band unchanged in the spectrum to show that the double absorption bands could be adjusted independently.

Figure 4 shows the performance of the double-band perfect sound absorber. In the simulation of Fig. 4(a), as the rotation angle of the cover cap changes from 0° to 315°, the central frequency of the upper absorption band is redshifted from 192 Hz to 176 Hz. During the tuning process, we find that the peak value of the upper absorption band is always close to unitary. Based on Eq. (4), we obtain that the acoustic impedance of the absorber keeps matched with the background air under the resonance condition, when the position of the opening aperture changes in the rotation. Figure 4(b) shows the results in our experiment, where the measurement data are plotted for every 45° rotations. The measurement result agrees well with the numerical simulation, where on the absorption spectrum, two separate absorption bands merge into a wide-band one after 315° rotation of the cover cap. In Figs. 4(c)–4(e), we further show the particle velocity fields at the rotation angles of 90°, 180° and 270°, with the frequencies at 191 Hz, 184 Hz and 176 Hz, respectively. The results reveal that at the operation frequencies for the three cases, local resonances take place with nontrivial particle velocity fields observed at the fan-like inner aperture, leading to a unitary sound absorption measured in experiments.

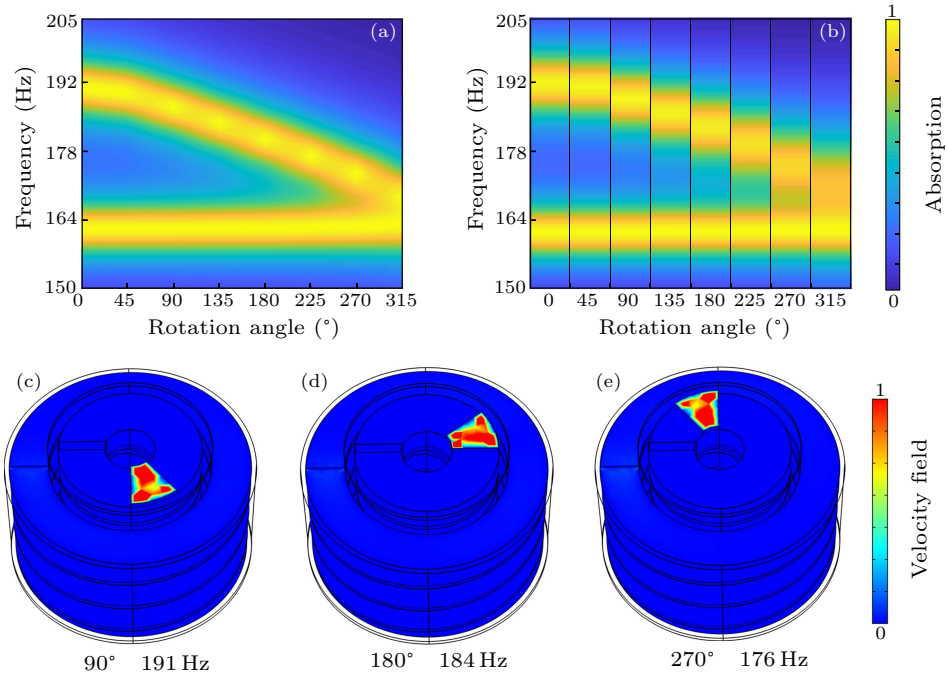


**Fig. 4.** [(a), (b)] The simulation and experimental measurement of sound absorption spectra at different rotation angles of the cover cap. [(c), (d), (e)] Simulated particle velocity fields at the rotation angles of 90°, 180° and 270°, with the corresponding resonance frequencies at 191 Hz, 184 Hz and 176 Hz, respectively.

In conclusion, we have designed a tunable double-band perfect absorber that operates at the local resonances in acoustic metasurfaces. The unit-cell comprises nesting helical tracks, which is a special type of 3D space coiling for high space utilization, and is featured with deep-subwavelength thicknesses for practical applications. We provide an effective and simple way to flexibly tune the absorption band in a spectrum without sacrificing the absorption intensity. We implement the tunable acoustic absorber and experimentally demonstrate its performance in wide-spectrum and adjustable sound absorption. Combined with the active control and artificial intelligence, our work will be promising for self-adaption flat acoustic devices,

such as intelligent acoustic meta-absorbers.

## References


[1] Biot M A 1962 *J. Acoust. Soc. Am.* **34** 1254
[2] Mei J, Ma G, Yang M, Yang Z, Wen W and Sheng P 2012 *Nat. Commun.* **3** 756
[3] Lee S H, Park C M, Seo Y M, Wang Z G and Kim C K 2010 *Phys. Rev. Lett.* **104** 054301
[4] Xiao S W, Ma G C, Li Y, Yang Z Y and Sheng P 2015 *Appl. Phys. Lett.* **106** 091904
[5] Ma G C, Yang M, Xiao S, Yang Z and Sheng P 2014 *Nat. Mater.* **13** 873
[6] Jiang X, Li Y and Zhang L K 2017 *J. Acoust. Soc. Am.* **141** EL363
[7] Zhao H, Wang Y, Yu D, Yang H, Zhong J, Wu F and Wen J 2020 *Compos. Struct.* **239** 111978
[8] Assouar M B, Senesi M, Oudich M, Ruzzene M and Hou Z 2012 *Appl. Phys. Lett.* **101** 173505
[9] Cai X, Guo Q, Hu G and Yang J 2014 *Appl. Phys. Lett.* **105** 121901
[10] Allard J F and Atalla N 2009 *Propagation of Sound in Porous Media: Modelling Sound Absorbing Materials* (Chichester: Wiley)
[11] Landau L D and Lifshitz E M 1986 *Course of Theoretical Physics: Theory of Elasticity* 3rd edn (Oxford: Butterworth-Heinemann)
[12] Zhang C and Hu X H 2016 *Phys. Rev. Appl.* **6** 064025
[13] Wang Y, Zhao H, Yang H, Zhong J, Zhao D, Lu Z and Wen J 2018 *J. Appl. Phys.* **123** 185109
[14] Xie Y B, Popa B I, Zigoneanu L and Cummer S A 2013 *Phys. Rev. Lett.* **110** 175501
[15] Liang Z X, Feng T H, Lok S K, Liu F, Ng K B, Chan C H, Wang J J, Han S, Lee S and Li J 2013 *Sci. Rep.* **3** 1614
[16] Li Y, Liang B, Gu Z M, Zou X Y and Cheng J C 2013 *Appl. Phys. Lett.* **103** 053505
[17] Liang Z and Li J 2012 *Phys. Rev. Lett.* **108** 114301
[18] Bongard F, Lissek H and Mosig J R 2010 *Phys. Rev. B* **82** 094306
[19] Li Y and Assouar B M 2016 *Appl. Phys. Lett.* **108** 063502
[20] Huang S B, Fang X S, Wang X, Assouar B M, Cheng Q and Li Y 2018 *Appl. Phys. Lett.* **113** 233501
[21] Li Y, Liang B, Tao Xu, Zhu X F, Zou X Y and Cheng J C 2012 *Appl. Phys. Lett.* **101** 233508
[22] Zhu X F, Li K, Zhang P, Zhu J, Zhang J T, Tian C and Liu S 2016 *Nat. Commun.* **7** 11731
[23] Ding Y H, Statharas E C, Yao K and Hong M 2017 *Appl. Phys. Lett.* **110** 241903
[24] Morse P M and Ingard K U 1987 *Theoretical Acoustics* (Princeton: Princeton University Press)
[25] Stinson M R 1991 *J. Acoust. Soc. Am.* **89** 550
[26] Ward G P, Lovelock R K, Murray A R J, Hibbins A P, Sambles J R and Smith J D 2015 *Phys. Rev. Lett.* **115** 044302